Proteomic Analysis of the Palmitate-induced Myotube Secretome Reveals Involvement of the Annexin A1-Formyl Peptide Receptor 2 (FPR2) Pathway in Insulin Resistance*[S]

Jong Hyuk Yoon‡, Dayea Kim‡, Jin-Hyeok Jang§, Jaewang Ghim‡, Soyeon Park‡, Parkyong Song‡, Yonghoon Kwon‡, Jaeyoon Kim‖, Daehee Hwang§¶‖‖, Yoe-Sik Bae‡‡, Pann-Ghill Suh§§, Per-Olof Berggren‖[a], and Sung Ho Ryu‡¶¶**

Elevated levels of the free fatty acid palmitate are found in the plasma of obese patients and induce insulin resistance. Skeletal muscle secretes myokines as extracellular signaling mediators in response to pathophysiological conditions. Here, we identified and characterized the skeletal muscle secretome in response to palmitate-induced insulin resistance. Using a quantitative proteomic approach, we identified 36 secretory proteins modulated by palmitate-induced insulin resistance. Bioinformatics analysis revealed that palmitate-induced insulin resistance induced cellular stress and modulated secretory events. We found that the decrease in the level of annexin A1, a secretory protein, depended on palmitate, and that annexin A1 and its receptor, formyl peptide receptor 2 agonist, played a protective role in the palmitate-induced insulin resistance of L6 myotubes through PKC-θ modulation. In mice fed with a high-fat diet, treatment with the formyl peptide receptor 2 agonist improved systemic insulin sensitivity. Thus, we identified myokine candidates modulated by palmitate-induced insulin resistance and found that the annexin A1-formyl peptide receptor 2 pathway mediated the insulin resistance of skeletal muscle, as well as systemic insulin sensitivity. ***Molecular & Cellular Proteomics 14: 10.1074/mcp.M114.039651, 882–892, 2015.***

The obesity epidemic has been linked to the development of metabolic complications such as hyperlipidemia, insulin resistance, and hypertension (1, 2). Hyperlipidemia/dyslipidemia involves abnormally elevated levels of lipids and/or lipoproteins in the plasma (3, 4). Obese patients exhibit characteristics of hyperlipidemia/dyslipidemia, such as abnormal elevations in plasma free fatty acid, cholesterol, and triglyceride levels, as well as a reduction in high-density lipoprotein content (3–5). Elevated free fatty acid levels in the plasma of obese patients play an important role in the development of insulin resistance (6). Hence, lowering the free fatty acid level in plasma has been shown to restore insulin sensitivity in these patients (7). Palmitate (C16:0) is a saturated free fatty acid found in animal plasma. It has been reported that the concentration of plasma palmitate in obese patients is higher than in healthy individuals (6, 8). In molecular studies, palmitate has been found to induce inflammation and insulin resistance in skeletal muscle cells by promoting diacylglycerol accumulation, which in turn activates protein kinase C (PKC)-θ[1] and NF-κB, leading to the inhibition of insulin-stimulated Akt phosphorylation through insulin receptor substrate 1 (IRS1) (S307) phosphorylation and IL-6 secretion (9). Sortilin was recently identified as a mediator of palmitate-dependent

From the ‡Department of Life Sciences, §School of Interdisciplinary Bioscience and Bioengineering, ¶Department of Chemical Engineering, Pohang University of Science and Technology (POSTECH), Pohang, Kyungbuk 790-784, Republic of Korea, ‖The Rolf Luft Research Center for Diabetes and Endocrinology, Karolinska Institutet, Stockholm SE-171 77, Sweden, **Department of Biological Science, Sungkyunkwan University, Suwon 440-746, Republic of Korea, ‡‡Samsung Advanced Institute for Health Sciences and Technology, Sungkyunkwan University, Seoul 135-710, Republic of Korea, §§School of Life Sciences, Ulsan National Institute of Science and Technology, Ulsan, 689-798, Republic of Korea, ‖‖Center for Plant Aging Research, Institute for Basic Science and Department of New Biology, Daegu Gyeongbuk Institute of Science and Technology, Daegu, 711-873, Republic of Korea, [a]Division of Integrative Biosciences and Biotechnology, Pohang University of Science and Technology (POSTECH), Pohang, Gyeongbuk, 790-784, Republic of Korea

Received, March 18, 2014 and in revised form, January 7, 2015
Published, MCP Papers in Press, January 23, 2015, DOI 10.1074/mcp.M114.039651
Author contributions: J.Y. and S.R. designed research; J.Y., D.K., J.J., J.G., S.P., P. Song, Y.K., J.K., D.H., and Y.B. performed research; J.Y., D.K., J.J., D.H., P. Suh, P.B., and S.R. analyzed data; J.Y. and S.R. wrote the paper.

[1] The abbreviations used are: APEX, absolute protein expression profiling; ERK, extracellular signal-regulated kinase; ESI, electrospray ionization; FPR2, formyl peptide receptor 2; GLUT4, glucose transporter type 4; GOBP, gene ontology biological process; GOCC, gene ontology cellular component; GTT, glucose tolerance test; HFD, high-fat diet; IRS1, insulin receptor substrate 1; LC, liquid chromatography; MS/MS, tandem mass spectrometry; NCD, normal chow diet; PKC, protein kinase C; Q-PCR, quantitative polymerase chain reaction; WAT, white adipose tissue.

insulin resistance, which regulates insulin-induced glucose transporter type 4 (GLUT4) trafficking (10). Therefore, palmitate is an important hyperlipidemic/dyslipidemic component that induces insulin resistance in skeletal muscle cells.

Skeletal muscle is thought to function as a tissue that produces and releases cytokines called myokines (11). As part of its extracellular signaling pathway, skeletal muscle secretes myokines that participate in myogenesis, angiogenesis, and nutrient generation in response to factors such as metabolic disorders, including insulin resistance, and exercise (11–13). Some myokines, including IL-6, IL-8, IL-15, and fibroblast growth factor 21, and brain-derived neurotrophic factor (14), are induced by exercise. Although myokines are thought to play a critical role in the regulation of (patho)physiological processes, few studies have investigated the role of myokine in metabolism. Because skeletal muscle has a major role in the regulation of glucose metabolism, it is important to identify putative crucial regulators, secreted from skeletal muscle, that modulate glucose metabolism by acting as autocrine/paracrine mediators as well as endocrine mediators (15).

Here, using an optimized secretomics approach, we performed a proteomic analysis of proteins in conditioned media from myotube cultures that were either untreated or treated with palmitate to induce insulin resistance (16, 17). Using a label-free quantitative analysis method, our aim was to characterize the skeletal muscle secretome and to identify skeletal muscle-derived proteins whose secretion is modulated by palmitate-induced insulin resistance. We found 36 putative secretory proteins modulated by palmitate-induced insulin resistance. The secretion of annexin A1 was down-regulated after palmitate treatment, and the annexin A1-formyl peptide receptor 2 (FPR2) pathway played a role in palmitate-induced insulin resistance in skeletal muscle by modulating the PKC-θ pathway.

EXPERIMENTAL PROCEDURES

Cell Culture and Establishment of Insulin Resistance—Rat L6 GLUT4myc skeletal myoblast cells were used to model skeletal muscle as previously described (17–21). Cells were cultured in the alpha formulation of minimum essential medium (α-MEM; Welgene, Daegu, Korea) supplemented with 10% FBS, 2 mM glutamine, 50 μg/ml streptomycin, and 50 μg/ml penicillin. Cells were provided by Dr. Amira Klip (Hospital for Sick Children, Toronto, Canada). The cells were passaged every second day, and confluency was maintained at less than 80% to prevent spontaneous differentiation. To induce differentiation, cells (4×10^4 cells/ml) were placed into α-MEM supplemented with 2% FBS for 5 days, with the medium refreshed every 48 h. The differentiation status was routinely monitored under a microscope (LSM 510 Meta; Zeiss, Germany). Sodium-palmitate (Sigma-Aldrich, St. Louis, MO) was dissolved in ethanol, heated to 50–60 °C for 30 min, and diluted in medium containing 2% serum (2% FBS in alpha-MEM) (22, 23). To induce palmitate-mediated insulin resistance, L6 myotubes were incubated with 150 μM of palmitate solution for 18 h in α-MEM supplemented with 2% FBS. Insulin resistance in primary mouse skeletal muscle cells (Cell Biologics Inc., Chicago, IL) was induced in the same way as described above for L6 cells.

Secretome Preparation for Mass Analysis—After the L6 myotubes were treated with palmitate, they were washed three times with completely unsupplemented α-MEM (no serum, phenol red, or antibiotics). Conditioned medium was prepared by incubated the myotubes with unsupplemented α-MEM for 5 h in a 37 °C CO_2 incubator. The conditioned medium was collected and centrifuged at 3500 rpm for 10 min (Combi-514R; Hanil Science Industry, Incheon, Korea). The resulting supernatant was collected and filtered using centrifugal filter units (cat# UFC900324; Millipore, MA) to eliminate contaminants. Dried samples filtered from the centrifugal filter units were reduced using 10 mM DTT in 50 mM ammonium bicarbonate and then alkylated with 100 mM iodoacetamide in 50 mM ammonium bicarbonate for tryptic digestion. Finally, each sample was treated with trypsin (Promega, Madison, WI) for 12 h at 37 °C and dried.

Mass Analysis and Database Searching—Tryptic digests (secretome peptides) were analyzed using a linear ion trap LTQ XL mass spectrometer (MS; Thermo, San Jose, CA) interfaced with a nanoelectrospray ion source. Chromatographic separation of peptides was achieved on a NanoLC·2D system (Eksigent, Dublin, CA) equipped with a 10-cm PicTip™ emitter with a 75-μm inner diameter (PF360–75-15-N-5; New Objective), packed in-house with a Magic C18AQ 5-μm/200-Å resin (Michrom Bioresources, Auburn, CA). Peptides were loaded from a cooled (4 °C) Eksigent auto-sampler and separated with a linear gradient of ACN/water, containing 0.1% formic acid, at a flow rate of 260 nl/min. Peptide mixtures were separated with a gradient of 2% to 40% ACN in 60 min. The analysis method consisted of a full MS scan with a range of 300–2000 *m/z* and data-dependent tandem mass spectrometry (MS/MS) on the five most intense ions from the full MS scan. The mass spectrometer was calibrated with the proposed calibration solution according to the manufacturer's instructions. This study used three biological replicates for each condition and two technical replicates for each biological replicate in the proteomic analysis.

The peak lists from the MS/MS data (RAW files) of the LTQ were generated using the Trans-Proteomic Pipeline (TPP, ver. 4.6.1) (24) and searched using a concatenated database that combined the International Protein Index (IPI) Rat FASTA database (ver. 3.85, 39,924 sequences; 21,245,823 residues) and Bovine FASTA database (ver. 3.73: 30,403 sequences; 16,412,134 residues) with the MASCOT search engine ver. 2.2.2 (Matrix Science, London, UK), selecting the Decoy database analysis. The MASCOT parameters allowed for tryptic specificity of up to two missed cleavages, with methylthio-modifications of cysteine as a fixed modification and oxidation of methionine as a variable modification. The LTQ search parameters for +1, +2, and +3 ions included mass error tolerances of ±2 Da for peptide ions and ±0.8 Da for fragment ions. In the MASCOT search results, when the significance threshold was set at 0.01, the individual ions score was more than 48 (supplemental Table S1). For the raw MASCOT search results, peptide-level (>95% probability) and protein-level (>99% probability) statistical validation was performed with PeptideProphet and ProteinProphet (25) in TPP. We removed frequently observed contaminants such as porcine trypsin, bovine proteins, and human keratins. Proteins supported by a single unique peptide were removed.

Label-free Quantitative Analysis Using Absolute Protein Expression Profiling (APEX)—APEX quantitation was performed using the APEX Quantitative Proteomics Tool ver. 1.1.0 (26). The APEX abundances of the proteins observed with liquid chromatography (LC)-MS/MS were calculated using the protXML files generated from the PeptideProphet and ProteinProphet analyses. An FDR of <5% was chosen, with a normalization factor of 1, which represents the total concentration of protein molecules.

Bioinformatic Analysis—Putative secretory proteins were selected using three independent methods. First, proteins with the Gene Ontology cellular components (GOCCs) of extracellular region or matrix were selected. Second, secretory proteins were identified based on signal sequence prediction. Following sequence extraction using an in-house program, the resulting FASTA file was loaded onto the SignalP 3.0 server (27) and processed using the "eukaryote" option; the search method was set to "Neural networks." Proteins with a D-score of >0.43 were then selected (16, 17). Third, secretory proteins were also identified based on nonclassical secretion prediction using SecretomeP 2.0 (28) as those with with an NN-score of >0.5 (16, 17). The DAVID software was used for functional enrichment analysis (http://david.abcc.ncifcrf.gov/) for Gene Ontology biological process (GOBP) and GOCC) A list of identified proteins was submitted and analyzed using the following parameters: the count threshold was set at 2, and the *p* value was set at 0.1 (a default cutoff) (16, 17). Putative exosomal proteins were screened using the ExoCarta exosome database (29).

Cell-based Stimulation Experiments—Following differentiation, L6 myotubes and primary mouse skeletal muscle cells were treated with 150 μM palmitate for 18 h to induce insulin resistance as described in the section detailing the "Cell culture and establishment of insulin resistance." The cells were cotreated with Ac2–26 (Anygen, Jangseong-gun, Jeonnam, Korea), WKYMVm (Trp-Lys-Tyr-Met-Val-D-Met; Anygen, Korea), WRW4 (Trp-Arg-Trp-Trp-Trp-Trp; Anygen), and palmitate for 18 h, depending on the experimental conditions. Then the cells were treated with 100 nM insulin for 20 min, and the cells were harvested.

Animal Experiments—All experimental procedures involving animals were approved by the POSTECH (Pohang University of Science and Technology) Animal Use and Care Committee. C57BL/6J mice (male, 6 weeks old) were kept under a 12-hour light/dark cycle with free access to water. The mice received a 60% high-fat diet (HFD) for 10 weeks to induce insulin resistance, and the body weight of each animal was monitored. WKYMVm was dissolved in a vehicle solution consisting of 20% water and 80% saline. After 10 weeks of a HFD, mice received intravenous injections of WKYMVm (200 μg/head) or vehicle daily for 5 days. For the glucose tolerance test (GTT), mice subjected to an overnight fast were injected intraperitoneally with glucose (1 g/kg). Blood was collected from the tail vein at 15, 30, 60, and 120 min, and glucose levels were measured. The fasting and feeding insulin levels were measured with an insulin ELISA kit (ALPCO). For lipid profiling, mouse serum was obtained by clotting the blood for 1 h, followed by centrifugation for 1 h at 2000 rpm. Serum triglyceride, cholesterol, LDL cholesterol, and high-density lipoprotein cholesterol were measured using an automatic chemistry analyzer (BS-380; Mindray). To observe insulin signaling in metabolic tissues, mice were fasted overnight; insulin was then injected intraperitoneally (5 units/kg) for 10 min. Phosphorylation of Akt in the skeletal muscles, liver, and epididymal white adipose tissue (WAT) was evaluated with Western blotting.

Statistical Analysis—All data were expressed as the mean ± S.E. All statistical analyses were performed using Student's *t* test (two groups) or one-way ANOVA (>two groups). Tukey's test or Tamhane's T2 test was used for multiple comparisons. A *p* value of <0.05 was considered significant.

(Experimental procedures for the GLUT4 translocation assay, the MTT assay, RNA extraction, quantitative PCR analysis, PCR analysis, and Western blot are presented in the supplemental Data).

RESULTS

Quantitative Proteomic Analysis of the Secretome of Palmitate-induced Insulin Resistance—To find appropriate conditions for palmitate-induced insulin resistance, we performed the GLUT4 translocation assay using differentiated L6 rat skeletal muscle cells treated with different concentrations of palmitate for 18 h. We found that 150–300 μM of palmitate inhibited insulin-induced GLUT4 translocation with statistical confidence (supplemental Fig. S1*A*). After measuring the cell viability (supplemental Fig. S1*B*), we selected 150 μM as the optimal concentration for insulin resistance. Treatment with 150 μM palmitate did not affect the morphology of L6 myotubes (Fig. 1*A*). After stimulating the cells with palmitate, we assessed the expression of pro-inflammatory cytokine genes, such as *TNF-α* and *IL-6*. The expression of *TNF-α* and *IL-6* increased under palmitate-treated conditions (Fig. 1*B*). To examine the possible impairment of downstream insulin-induced signaling after palmitate treatment, we used Western blotting to monitor the phosphorylation of Akt, an important signaling molecule in insulin stimulation. Insulin-induced phosphorylation of Akt (S473) was markedly inhibited after palmitate treatment (Fig. 1*C*).

For the secretome analysis, we collected and processed conditioned media from palmitate-treated and nontreated (NT) cells. The trypsin-digested peptides from the conditioned medium were subjected to LC- electrospray ionization (ESI)-MS/MS. We searched the combined rat/bovine IPI database using the MASCOT search engine and identified 189 proteins from NT and palmitate-treated conditions (Fig. 1*D* and supplemental Table S1). We used APEX for label-free protein quantification (26) and found that the abundances of 36 proteins had changed (p value < 0.05 and $\log_2$ change > 0.58): the levels of eight proteins were higher in the palmitate-treated group than in the NT control, whereas those of 28 proteins were lower (supplemental Table S1). To select putative secretory proteins from among these proteins, we used a previously reported approach that utilizes three separate methods (16, 17). Among the 36 proteins modulated by palmitate-induced insulin resistance, Gene Ontology selected 21 proteins, signal sequence prediction selected 25 proteins, and nonclassical secretion prediction selected six proteins as secretory proteins. Twelve exosomal proteins were screened with the ExoCarta database. Thus, 36 proteins were selected as secretory proteins modulated by palmitate-induced insulin resistance (Table I).

To verify the quantitative results, we analyzed several representative proteins secreted after palmitate treatment with quantitative polymerase chain reaction (Q-PCR) and Western blotting. Q-PCR analysis showed that the gene expression of two secretory proteins, including heat shock protein beta-1 (Hspb1) and serpin H1 (Serpinh1), increased markedly; however, the level of collagen alpha-1(I) chain (Col1a1) decreased (Fig. 1*E*). These results correlated with the results of the LC-ESI-MS/MS analysis. Western blot analysis also showed that the levels of two secretory proteins, matrix metalloproteinase-2 (MMP-2) and annexin A1, decreased in the palmitate-treated samples, a result that was also consistent with the results of the LC-ESI-MS/MS analysis (Fig. 1*F*).

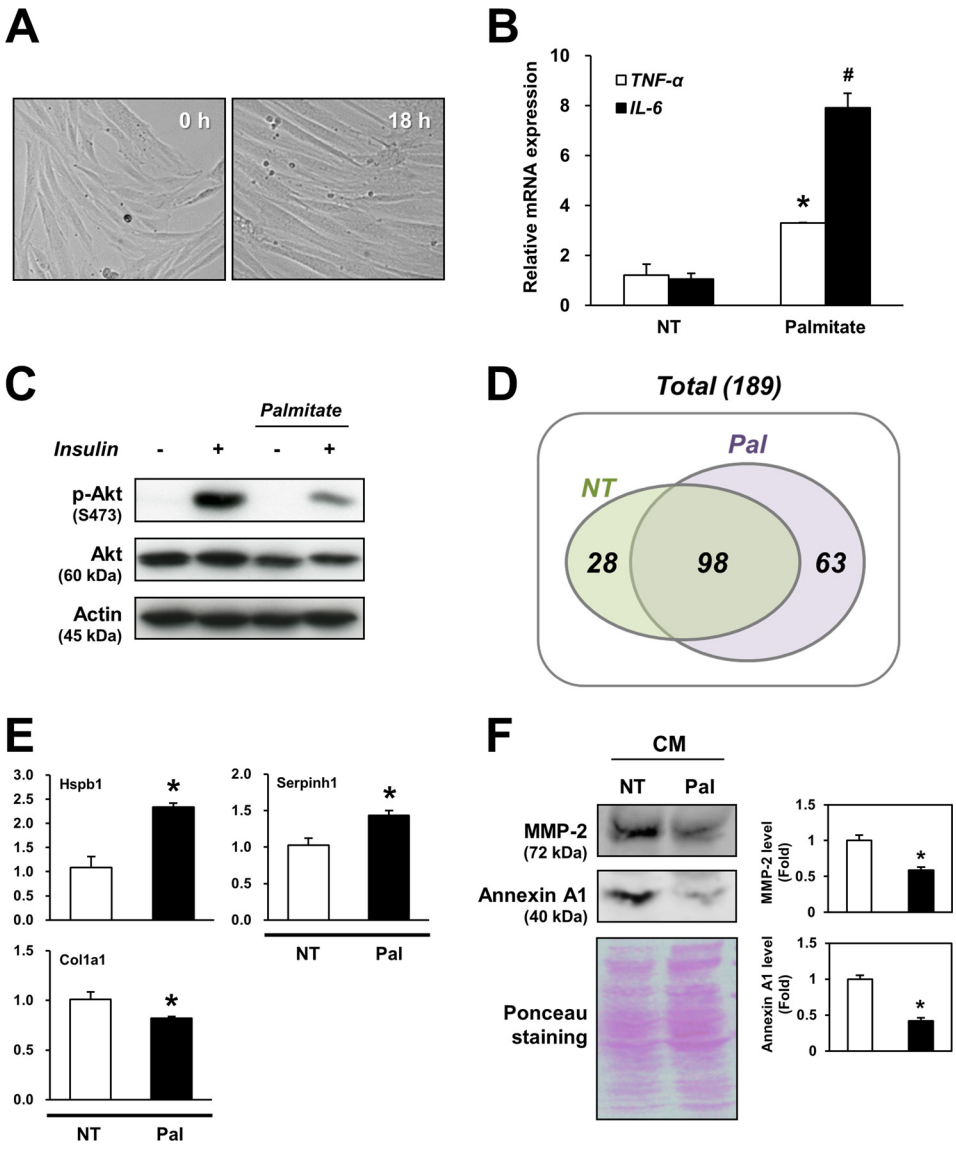

FIG. 1. **Conditioned media preparation and quantitative proteomic analysis of the palmitate-induced insulin resistance secretome.** *A*, Microscopic images of differentiated L6 rat skeletal muscle cells. Sequential optical microscopy images indicate L6 rat skeletal muscle cells after palmitate treatment. *B*, Q-PCR analysis of *TNF-α* and *IL-6*. The *y* axis indicates fold change relative to the NT control. *, $^{\#}p < 0.05$, between NT and palmitate condition. *C*, Western blot of proteins that mediate insulin downstream signals. Conditioned cell lysates were electrophoresed and blotted. "Insulin" indicates 100 nM of insulin treatment for 20 min. *D*, Venn diagram of the 189 identified proteins. "NT" and "Pal" indicate the control and palmitate-treated conditions, respectively. *E*, Q-PCR analysis of palmitate-modulated secretory proteins. The *y* axis indicates the relative fold change against the NT control. *F*, Western blots of palmitate-modulated secretory proteins. The levels of MMP-2 and annexin A1 decreased in the conditioned media of palmitate condition. "CM" indicates conditioned media from both conditions. "NT" and "Pal" indicate the control and palmitate-treated conditions, respectively. The right graphs show densitometric analysis of MMP-2 and annexin A1. Western blot results were densitometrically analyzed using ImageJ (ver. 1.38). All data in the figure are presented as mean ± S.E., $n = 3–4$ per group; *, $^{\#}p < 0.05$, in the Student's *t* test.

Bioinformatic Analysis of Secretory Proteins Modulated by Palmitate-induced Insulin Resistance—To identify the biological features of the increased and decreased proteins, we used the DAVID software (16, 17). Enrichment analysis of GOBPs revealed that the increased proteins were involved in cellular homeostasis, actin filament organization, and regulation of apoptosis, whereas the decreased proteins were involved in cell adhesion, extracellular matrix organization, response to wounding, and regulation of cell growth (supplemental Fig. S2*A*). The analysis of GOCCs showed that, interestingly, only the decreased proteins predominantly localized to the extracellular region, whereas the increased proteins predominantly localized to intracellular regions (supplemental Fig. S2*B*). Additionally, we studied the secretory proteins using two recent reports that provided lists of known stress proteins or proteins repeatedly identified in proteomic analy-

TABLE I

List of secretory proteins modulated by Palmitate-induced insulin resistance. For "Filtering methods," letters indicate how proteins were identified as secretory: "G" indicates Gene Ontology, "C" indicates SignalP (Classical), "N" indicates SecretomeP (Nonclassical) and "E" indicates ExoCarta (Exosome). "Fold change" indicates change of value of APEX for each protein between NT and Palmitate condition

Accession	Name	Filtering methods	Fold change (log2)	*p* value
IPI00958044.1	Histone cluster 1, H2ae-like	N	1.59	0.0026
IPI00324741.3	Protein disulfide-isomerase A3	C,E	0.87	0.0000
IPI00230941.5	Vimentin	N,E	0.83	0.0000
IPI00231260.5	Peroxiredoxin-6	E	0.73	0.0278
IPI00201586.1	Heat shock protein beta-1	N,E	0.72	0.0015
IPI00204703.5	Serpin H1	C	0.69	0.0002
IPI00231734.5	Fructose-bisphosphate aldolase A	E	0.62	0.0003
IPI00327144.7	Cofilin-1	N,E	0.61	0.0362
IPI00188909.3	Collagen alpha-1(I) chain	G,C	−0.59	0.0094
IPI00361798.2	Insulin-like growth factor binding protein 7	G,C	−0.70	0.0002
IPI00194566.1	Procollagen C-endopeptidase enhancer 1	G,C	−0.73	0.0000
IPI00207199.3	Connective tissue growth factor	G,C	−0.73	0.0039
IPI00205807.1	Metalloproteinase inhibitor 2	G,C	−0.81	0.0002
IPI00197696.2	Malate dehydrogenase, mitochondrial	E	−0.82	0.0000
IPI00231615.5	Annexin A1	G,E	−0.91	0.0149
IPI00189714.5	Collagen, type XII, alpha 1	G,N	−0.99	0.0238
IPI00476991.1	Neural cell adhesion molecule 1	C	−1.03	0.0000
IPI00191090.1	Biglycan	G,C	−1.09	0.0000
IPI00194930.5	Glypican-1	G,C	−1.13	0.0000
IPI00204359.1	Beta-2-microglobulin	G,C,E	−1.18	0.0000
IPI00188921.1	Collagen alpha-2(I) chain	G,C	−1.19	0.0000
IPI00189424.2	SPARC	G,C	−1.23	0.0000
IPI00191578.4	72 kDa type IV collagenase (MMP-2)	G,C	−1.29	0.0009
IPI00326070.3	Cathepsin L1	G,C	−1.31	0.0000
IPI00205022.1	Nucleobindin-1	C	−1.38	0.0000
IPI00758468.2	Plasma glutamate carboxypeptidase	G,C	−1.39	0.0014
IPI00206239.1	Insulin-like growth factor-binding protein 4	G,C	−1.43	0.0026
IPI00326433.11	10 kDa heat shock protein, mitochondrial	N	−1.44	0.0236
IPI00197074.3	Dystroglycan 1	G,C	−1.56	0.0003
IPI00373753.5	Protein tyrosine kinase 7	E	−1.56	0.0001
IPI00411254.1	M-cadherin	C	−1.60	0.0000
IPI00210920.1	Aspartate aminotransferase, mitochondrial	C	−1.66	0.0001
IPI00364868.3	collagen, type XV, alpha 1	G,C	−1.72	0.0000
IPI00366944.2	Collagen alpha-1(III) chain	G,C,E	−2.03	0.0000
IPI00200757.1	Isoform 1 of Fibronectin	G,C,E	−2.37	0.0000
IPI00366945.3	collagen, type V, alpha 2	G,C	−2.43	0.0018

ses (30, 31). We found that ~62% of the increased secretory proteins overlapped with the proteins in these lists, indicating that they are stress proteins (supplemental Fig. S2*C*). In contrast, only ~7% of the decreased secretory proteins were on these lists. The bioinformatics results indicate a clear difference in the functional annotation pattern and biological characteristics of the increased and decreased secretory proteins. They also suggest that functional cytokine candidates are present among the decreased proteins rather than among the increased proteins.

Protective Role of Annexin A1 and its Receptor Agonist (WKYMVm) in Palmitate-Induced Insulin Resistance in L6 Myotubes—From the results of the bioinformatics study, we hypothesized that the group of decreased proteins included functional cytokine candidates. In the proteomics study, we found that annexin A1 decreased in the secretome of palmitate-treated cells (Table I), and we confirmed that its secretion was down-regulated in conditioned media (Fig. 1*F*). Furthermore, it has been reported that the plasma level of annexin A1 is down-regulated in obese patients (32). Recent reports on the anti-inflammatory effect of annexin A1 and the relationship between inflammation and insulin resistance (33) led us to investigate the putative role of annexin A1 as a regulator of insulin resistance in skeletal muscle. Because previous reports have demonstrated that annexin A1 acts on an important chemoattractant receptor, FPR2 (34, 35), we investigated whether L6 skeletal muscle cells express the annexin A1 receptor. As shown in supplemental Fig. S3*A*, L6 skeletal muscle cells expressed FPR2 at the mRNA level. Stimulation of the cells with an N-terminal-derived active peptide of annexin A1, Ac2–26, and a well-characterized FPR2 agonist, WKYMVm, elicited ERK (extracellular signal-regulated kinase) phosphorylation, indicating that L6 skeletal muscle cells expressed the functional annexin A1 receptor, FPR2

(supplemental Fig. S3*B* and S3*C*). Insulin-induced Akt phosphorylation is a crucial component of insulin signaling. However, insulin-induced Akt phosphorylation was strongly inhibited when cells were exposed to palmitate for 18 h (Fig. 2*A*). When the cells were stimulated with Ac2–26 in the presence of palmitate, palmitate-induced insulin resistance was markedly reduced. Ac2–26 alone did not affect insulin-induced Akt phosphorylation in the absence of palmitate. To determine if FPR2 agonists in general have an inhibitory effect on palmitate-induced insulin resistance, we tested the effect of the FPR2 agonist WKYMVm in the system. In addition to Ac2–26, WKYMVm strongly blocked palmitate-induced insulin resistance, with increased levels of Akt phosphorylation observed in the presence of palmitate (Fig. 2*B*). These results indicate that the annexin A1-FPR2-mediated signaling pathway protects L6 myotubes from the palmitate-induced impairment of downstream insulin signaling.

It has been reported that palmitate induces insulin resistance through the phosphorylation of PKC-θ at T538 and that phosphorylated PKC-θ induces IRS1 phosphorylation at S307, as well as IL-6 expression (9). We further investigated the involvement of the annexin A1-FPR2 axis in palmitate-induced insulin resistance in L6 myotubes. We found that Ac2–26 inhibited the phosphorylation of PKC-θ (T538) and IRS1 (S307) in the presence of palmitate (Fig. 2*C*). The FPR2 agonist WKYMVm also inhibited the phosphorylation of PKC-θ and IRS1 under the same conditions (Fig. 2*D*). We then assessed the expression of IL-6, another downstream target of PKC-θ. Both Ac2–26 and WKYMVm reduced IL-6 expression in L6 myotubes (Fig. 2*E*).

Next, using a well-characterized FPR2 antagonist, WRW4 (Trp-Arg-Trp-Trp-Trp-Trp) (36–38), we determined whether modulation of FPR2 activity inhibits the protective effect of WKYMVm. When cells were cotreated with WRW4 in the presence of WKYMVm, the insulin-dependent phosphorylation of Akt was lower than after treatment with WKYMVm alone (supplemental Fig. S4*A*). We then evaluated the effect of WRW4 on the phosphorylation of PKC-θ (T538) and IRS1 (S307) in the presence of palmitate. We found that WRW4 treatment inhibited the WKYMVm-induced reduction in PKC-θ (T538) and IRS1 (S307) phosphorylation (supplemental Fig. S4*B*). We also assessed the protective effect of WKYMVm in primary mouse skeletal muscle cells. Treatment with WKYMVm blocked palmitate-induced insulin resistance; Akt phosphorylation increased in the presence of palmitate (supplemental Fig. S5*A*). WKYMVm also inhibited the phosphorylation of PKC-θ (T538) and IRS1 (S307) under the same conditions (supplemental Fig. S5*B*). These results indicated that modulation of FPR2 inhibited the protective effect of WKYMVm on palmitate-induced insulin resistance. Collectively, these findings suggest that the annexin A1-FPR2 axis alters insulin resistance in skeletal muscle by modulating the PKC-θ pathway.

Improvement of Insulin Sensitivity in High-fat Diet Mice after Treatment with an FPR2 Agonist—We hypothesized that annexin A1 plays a protective role in preventing insulin resistance in the metabolically normal state. However, in obesity, lower plasma levels of annexin A1 contribute to the development of insulin resistance. Therefore, we expected that annexin A1 would be involved in a relatively early stage of insulin resistance. To investigate the *in vivo* role of annexin A1 in the early stages of insulin resistance, we fed C57BL/6J mice a HFD for 10 weeks. Body weight increased significantly, indicative of an obese state (supplemental Fig. S6*A*). We measured annexin A1 levels in the plasma as well as in the lysates of skeletal muscle. The plasma level of annexin A1 was markedly lower in HFD mice than in normal chow diet (NCD) mice (Fig. 3*A*). This result correlated with the quantitative secretomics data obtained using palmitate-treated cells (Table I). The level of annexin A1 in skeletal muscle was also down-regulated in HFD mice (supplemental Fig. S6*B*). Because we identified a protective role for the annexin A1-FPR2 axis in palmitate-induced insulin resistance, we further characterized its effect on whole-body insulin sensitivity in NCD and HFD mice. We intravenously injected the FPR2 agonist WKYMVm into NCD and HFD mice for 5 days and measured metabolic changes. During the injection period, there was no significant change in body weight (supplemental Fig. S6*C*). When we performed GTTs (Fig. 3*B*), we noted a clear improvement in glucose tolerance in HFD mice at 30 and 60 min following glucose injection. The area under the curve (AUC) for the GTT also decreased in the treatment groups (supplemental Fig. S7*A*). The increase in fasting glucose level was not statistically significant in HFD mice treated with the FPR2 agonist (Fig. 3*C*). The FPR2 agonist clearly reduced the fasting insulin level in HFD mice (Fig. 3*D*), as well as the feeding glucose and insulin levels (supplemental Fig. S7*B* and S7*C*).

Effects of the Annexin A1 Receptor Agonist on Metabolic Tissues in HFD Mice—We further characterized the insulin sensitizing effects of the annexin A1 receptor agonist on metabolic tissues in HFD mice. The phosphorylation of PKC-θ and IRS1 in skeletal muscle tissue was examined with Western blot to determine whether the results were consistent with those from L6 myotubes. Administration of the FPR2 agonist reduced the phosphorylation of PKC-θ (T538) and IRS1 (S307) in HFD mice (Fig. 4*A*). We further investigated whether administration of the FPR2 agonist improved insulin-stimulated Akt phosphorylation in metabolic tissues. In the case of skeletal muscle, insulin-stimulated Akt phosphorylation (S473) was higher in HFD mice administered the FPR2 agonist than in HFD mice administered vehicle alone (Fig. 4*B*). Insulin-stimulated Akt phosphorylation in the liver also increased (for the same comparison). However, there was no significant change in Akt phosphorylation in WAT.

Insulin resistance is associated with a change in the cytokine profile of WAT (39). Here, we compared the mRNA levels of several important inflammatory cytokines, such as TNF-α,

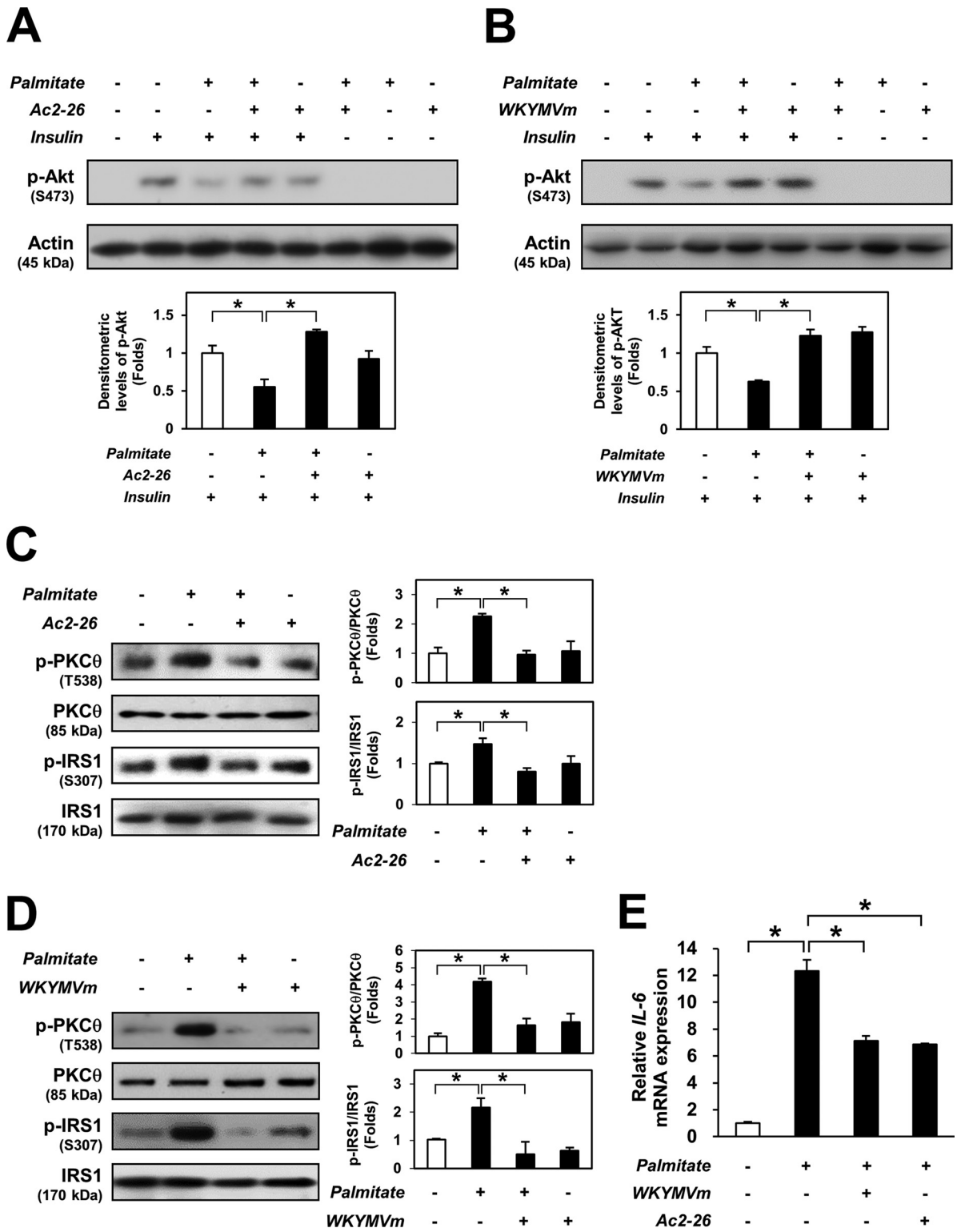

FIG. 2. **Protective role of annexin A1 and its receptor agonist, WKYMVm, on palmitate-induced insulin resistance of L6 myotubes.** *A*, Western blot of Akt phosphorylation after cotreatment with 150 μM palmitate and 10 μM Ac2–26. Conditioned cell lysates were electrophoresed and blotted. The lower graph shows densitometric analysis of Akt phosphorylation. *B*, Western blot of Akt phosphorylation after cotreatment with 150 μM palmitate and 100 nM WKYMVm. Conditioned cell lysates were electrophoresed and blotted. The lower graph shows densitometric analysis of Akt phosphorylation. "Insulin" indicates 100 nM of insulin treatment for 20 min. *C*, Western blot of PKC-θ and IRS1 phosphorylation after cotreatment with 150 μM palmitate and 10 μM Ac2–26. Conditioned cell lysates were electrophoresed and blotted. The right graph shows

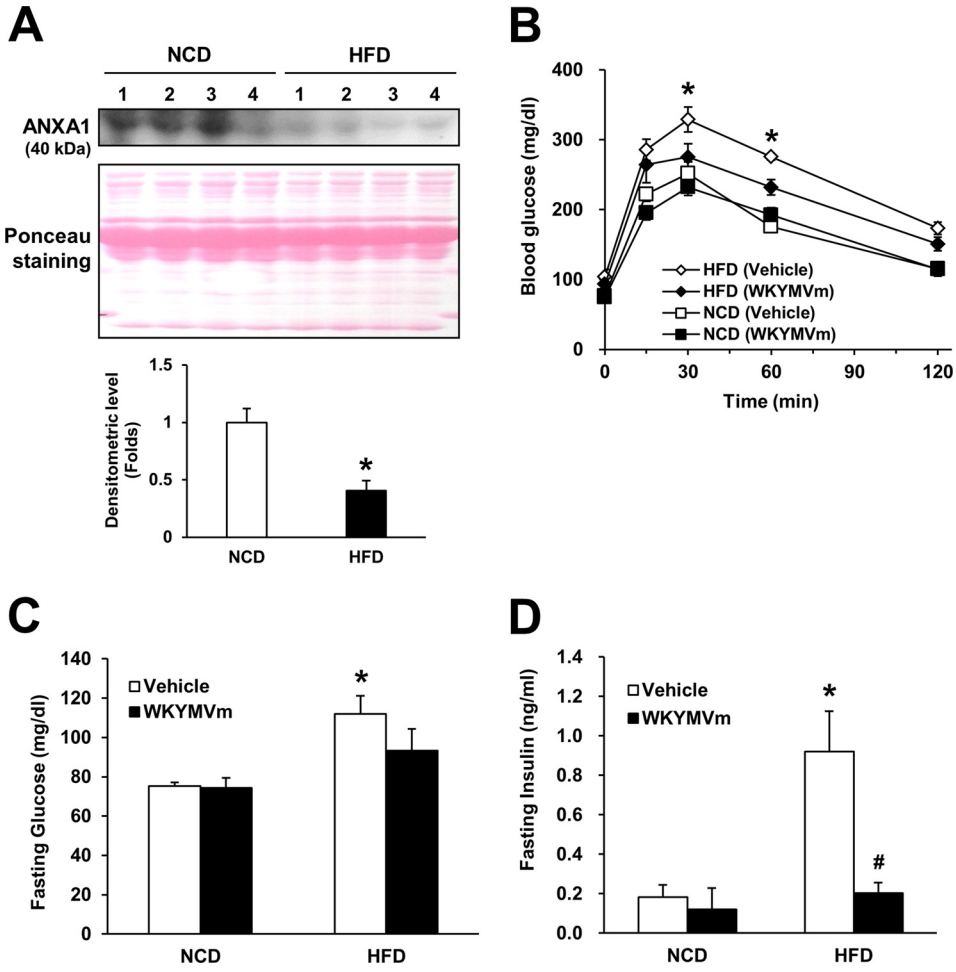

FIG. 3. **Improvement of insulin sensitivity by treatment of the annexin A1 receptor agonist in HFD mice.** Mice were fed an NCD or HFD for 10 weeks, and then treated with 200 μg/head of WKYMVm or a vehicle control for 5 days. *A*, Western blot of annexin A1 in the plasma of vehicle-treated NCD or HFD mice. The lower graph shows densitometric analysis of annexin A1. ANXA1 indicates annexin A1. *B*, Glucose tolerance test for the treatment groups. $^{*}p < 0.05$, between HFD (Vehicle) and HFD (WKYMVm). *C*, Fasting plasma glucose concentrations in each treatment group. $^{*}p < 0.05$, between NCD (Vehicle) and HFD (Vehicle). *D*, Fasting plasma insulin concentrations in each treatment group. $^{*}p < 0.05$, between NCD (Vehicle) and HFD (Vehicle). $^{\#}p < 0.05$, between HFD (Vehicle) and HFD (WKYMVm). All data in the figure are presented as mean ± S.E.; $n = 3{\sim}5$ per group; *, $^{\#}p < 0.05$, in Student's *t* test or in one-way ANOVA.

IL-1β, CCL2, and IL-4, in the WAT of HFD mice after administration of vehicle or FPR2 agonist (Fig. 4*C*). The mRNA expression of *TNF-*α, *IL-1*β, and *CCL2* was down-regulated by the FPR2 agonist. However, the level of *IL-4* mRNA increased in mice administered the FPR2 agonist. There were no significant changes in the mRNA levels of these cytokines in NCD mice (supplemental Fig. S7*D*). In addition, we profiled representative serum lipids, including triglyceride, cholesterol, LDL cholesterol, and high-density lipoprotein cholesterol. There were no significant differences between vehicle and WKYMVm treatment (supplemental Fig. S8). These results indicate that the FPR2 agonist WKYMVm improves insulin sensitivity in HFD mice by sensitizing the insulin pathway in metabolic tissues, including skeletal muscle and the liver, and by regulating inflammatory cytokine expression in WAT.

DISCUSSION

To our knowledge, this is the first proteomic study of conditioned media following the development of palmitate-induced insulin resistance in skeletal muscle. Using optimized

densitometric analysis of PKC-θ and IRS1 phosphorylation. *D*, Western blot of PKC-θ and IRS1 phosphorylation after cotreatment with 150 μM palmitate and 100 nM WKYMVm. Conditioned cell lysates were electrophoresed and blotted. The right graph shows densitometric analysis of PKC-θ and IRS1 phosphorylation. Western blot results were densitometrically analyzed using ImageJ (ver. 1.38). *E*, Relative mRNA expression of IL-6 after cotreatment with 150 μM palmitate and 10 μM Ac2–26 or 100 nM WKYMVm. The *y*-axis indicates the relative fold change against the nontreated control. All data in the figure are presented as mean ± S.E. $n = 3$–5 per group; $^{*}p < 0.05$ in Student's *t* test or in one-way ANOVA.

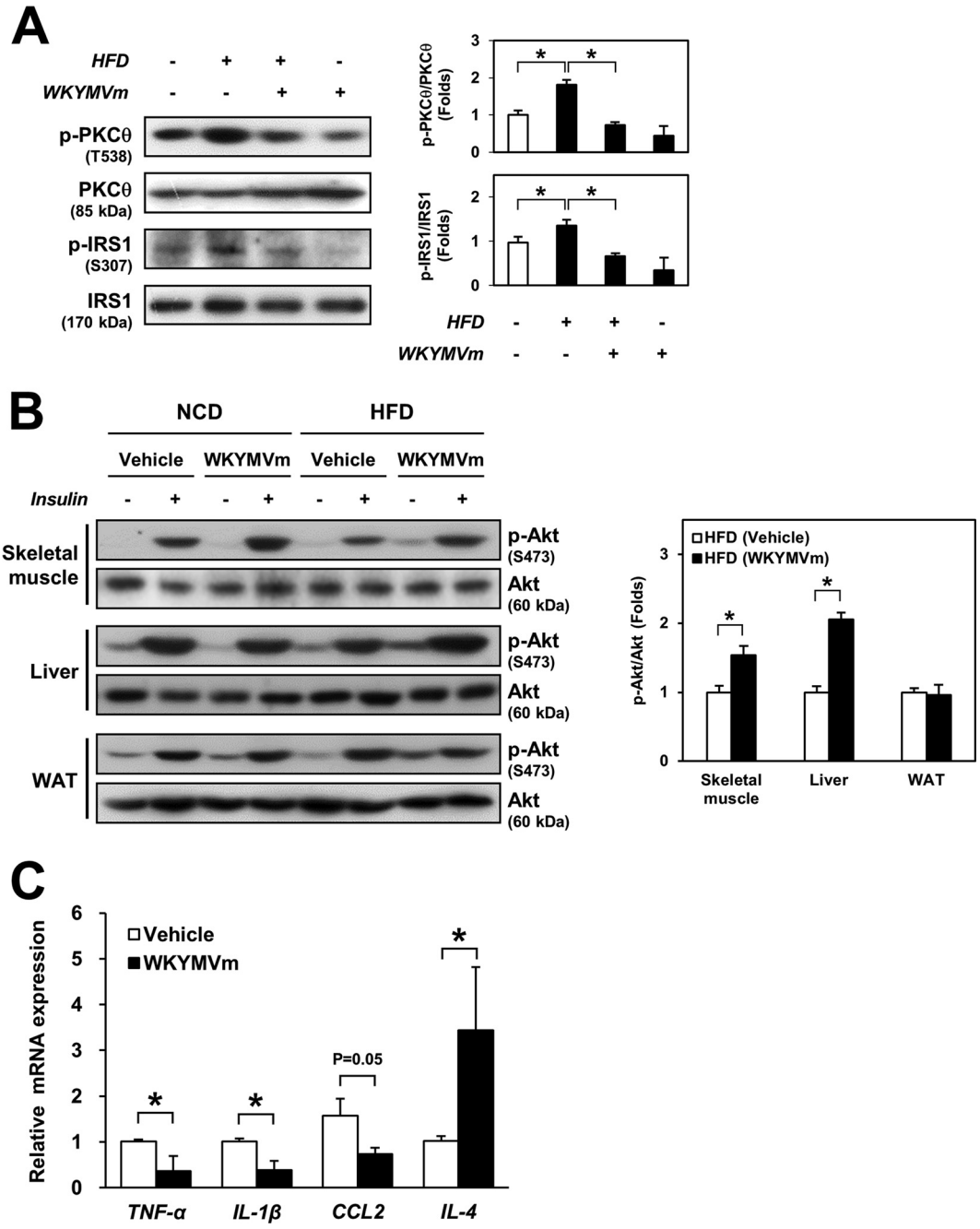

FIG. 4. **Effects of the annexin A1 receptor agonist on metabolic tissues in HFD mice.** Mice were fed an NCD or HFD for 10 weeks, and then treated with 200 μg/head of WKYMVm or a vehicle control for 5 days. *A*, Western blot of PKC-θ and IRS1 in skeletal muscle from HFD mice administered the FPR2 agonist. Conditioned tissue lysates were electrophoresed and blotted. The right graph shows densitometric analysis of PKC-θ and IRS1 phosphorylation. *B*, Western blot of Akt phosphorylation of metabolic tissues, including skeletal muscles, the liver, and WAT, after intraperitoneal injection of insulin (5 U/kg) for 10 min. Conditioned tissue lysates were electrophoresed and blotted. The right graph shows densitometric analysis of Akt phosphorylation. Western blot results were densitometrically analyzed using ImageJ (ver. 1.38). *C*, Relative mRNA expression of inflammatory cytokines in the WAT of HFD mice: *TNF-α*, *IL-1β*, *CCL2*, and *IL-4*. All data in the figure are presented as mean ± S.E.; $n = 3\sim5$ per group; $^{*}p < 0.05$, in Student's *t* test or in one-way ANOVA.

secretomic techniques, we identified 189 skeletal muscle-derived proteins in the conditioned media. Using a reliable, label-free quantitative method and a secretory protein filtering method, we found 36 putative secretory proteins that were modulated by palmitate-induced insulin resistance. We have provided a list of new myokine candidates, which is valuable information for designing further diabetes studies. We have also identified biomarkers for obesity-induced insulin resistance. In

particular, we found that secretion of the myokine annexin A1 decreased under conditions that induced palmitate-induced insulin resistance. Through subsequent cell and animal experiments, we found that the annexin A1-FPR2 pathway played a role in the palmitate-induced insulin resistance of L6 myotubes, as well as in systemic insulin resistance.

Annexin A1, the first well-characterized member of the annexin family, is a calcium-dependent phospholipid-binding protein (40). Annexin A1 regulates diverse cellular processes, including vesicle trafficking, cytoskeletal rearrangement, cell migration, and inflammation (40). In skeletal muscle physiology, annexin A1 promotes the migration of muscle satellite cells, resulting in myoblast cell differentiation (41). The target receptor for annexin A1, FPR2, an important classical chemoattractant receptor, mediates leukocyte recruitment and anti-inflammatory effects induced by an N-terminal-derived peptide of annexin A1, Ac2–26 (33). Although the plasma level of annexin A1 is down-regulated in obese patients (32), its metabolic function as a cytokine and its mode of action have not been characterized. Here, we describe a putative role for annexin A1 in the insulin resistance of skeletal muscle cells. Annexin A1 and WKYMVm, which act on the same receptor, FPR2, strongly blocked palmitate-induced insulin resistance, restoring insulin-induced signaling *in vitro*. WKYMVm ameliorated HFD-induced insulin resistance in mice. Annexin A1 is involved in the anti-inflammatory pathway and is down-regulated in the plasma of obese patients (32, 33). We have also reported that the annexin A1 level decreases in the myotube secretome of TNF-α-induced insulin resistance (17). Considering these findings, it is possible that the secretion of annexin A1 decreases in major cases of insulin resistance involving inflammation and hyperlipidemia. As a novel myokine, annexin A1 might serve as an auto/endocrine mediator that regulates insulin resistance.

Here, we showed that activation of FPR2 improves key metabolic features in HFD mice. This effect was observed only in the HFD condition, not in the NCD condition. Furthermore, activation of FPR2 inhibited proinflammatory cytokines and induced anti-inflammatory cytokines in WAT. Thus, activation of FPR2 in HFD mice reversely regulates whole-body inflammation, which is a well-known cause of metabolic disease. In support of this idea, it was previously reported that FPR2-knockout mice show signs of marked inflammation, including increased cell adherence and emigration in the mesenteric microcirculation following an ischemia-reperfusion insult, and an augmented acute response to carrageenan-induced paw edema (34). To understand the function of annexin A1 as a myokine, the use of conditional mouse models, such as skeletal muscle-specific knockout mice, will be important for future work.

According to the series of bioinformatic studies shown in Fig. 2, the functional annotation features of proteins that increased and decreased differed. It has been reported that palmitate-induced cellular stress is mediated by a well-known pathway, including the diacylglycerol-PKC-NF-κB axis (42–45). We found that approximately half of the increased proteins were stress proteins. This indicates that palmitate treatment induces cellular stress and the secretion of stress-related proteins. In contrast, the decreased proteins were annotated as extracellular proteins, and they included fewer stress proteins. This suggests that palmitate-induced insulin resistance affects the secretion of candidate myokines, particularly those whose secretion was reduced. The results also validated our experimental set-up by showing that palmitate induces insulin resistance through cellular stress.

In conclusion, we used a reliable and optimized proteomic approach to identify myokine candidates produced by skeletal muscle in response to palmitate-induced insulin resistance. We found that annexin A1 secretion was down-regulated and that the annexin A1-FPR2 pathway played a protective role in palmitate-induced insulin resistance in L6 myotubes by modulating the PKC-θ pathway. Treatment of HFD mice with the FPR2 agonist significantly improved whole-body insulin sensitivity by sensitizing the insulin pathway in metabolic tissues, including skeletal muscle and the liver, and by regulating inflammatory cytokine expression in WAT. Thus, the annexin A1-FPR2 axis might be a new therapeutic target for insulin resistance.

* This work was supported by a National Research Foundation of Korea (NRF) grant funded by the Korean government (MEST) (No. 2013R1A2A1A03010110) and Institute for Basic Science (IBS-R013-G1-2014-a00), Republic of Korea.

S This article contains supplemental Figs. S1 to S8, Table S1, and Data.

¶¶ To whom correspondence should be addressed: Department of Life Sciences, POSTECH Biotech Center, Pohang University of Science and Technology (POSTECH), San 31 Hyojadong, Pohang 790-784, Republic of Korea. Tel.: +82-54-279-2292; Fax: +82-54-279-0645; E-mail: sungho@postech.ac.kr.

REFERENCES

1. Moller, D. E., and Kaufman, K. D. (2005) Metabolic syndrome: a clinical and molecular perspective. *Annu. Rev. Med.* **56,** 45–62
2. Coenen, K. R., and Hasty, A. H. (2007) Obesity potentiates development of fatty liver and insulin resistance, but not atherosclerosis, in high-fat diet-fed agouti LDLR-deficient mice. *Am. J. Physiol. Endocrinol. Metab.* **293,** E492–E499
3. Arsenault, B. J., Boekholdt, S. M., and Kastelein, J. J. (2011) Lipid parameters for measuring risk of cardiovascular disease. *Nat. Rev. Cardiol.* **8,** 197–206
4. Brandt, M. L., Harmon, C. M., Helmrath, M. A., Inge, T. H., McKay, S. V., and Michalsky, M. P. (2010) Morbid obesity in pediatric diabetes mellitus: surgical options and outcomes. *Nat. Rev. Endocrinol.* **6,** 637–645
5. Loria, P., Carulli, L., Bertolotti, M., and Lonardo, A. (2009) Endocrine and liver interaction: the role of endocrine pathways in NASH. *Nat. Rev. Gastroenterol. Hepatol.* **6,** 236–247
6. Coll, T., Palomer, X., Blanco-Vaca, F., Escola-Gil, J. C., Sanchez, R. M., Laguna, J. C., and Vazquez-Carrera, M. (2010) Cyclooxygenase 2 inhibition exacerbates palmitate-induced inflammation and insulin resistance in skeletal muscle cells. *Endocrinology* **151,** 537–548
7. Barma, P., Bhattacharya, S., Bhattacharya, A., Kundu, R., Dasgupta, S., Biswas, A., Bhattacharya, S., Roy, S. S., and Bhattacharya, S. (2009) Lipid induced overexpression of NF-kappaB in skeletal muscle cells is linked to insulin resistance. *Biochim. Biophys. Acta* **1792,** 190–200
8. Zhang, X. J., Chinkes, D. L., Aarsland, A., Herndon, D. N., and Wolfe, R. R.

(2008) Lipid metabolism in diet-induced obese rabbits is similar to that of obese humans. *J. Nutr.* **138,** 515–518
9. Coll, T., Eyre, E., Rodriguez-Calvo, R., Palomer, X., Sanchez, R. M., Merlos, M., Laguna, J. C., and Vazquez-Carrera, M. (2008) Oleate reverses palmitate-induced insulin resistance and inflammation in skeletal muscle cells. *J. Biol. Chem.* **283,** 11107–11116
10. Tsuchiya, Y., Hatakeyama, H., Emoto, N., Wagatsuma, F., Matsushita, S., and Kanzaki, M. (2010) Palmitate-induced down-regulation of sortilin and impaired GLUT4 trafficking in C2C12 myotubes. *J. Biol. Chem.* **285,** 34371–34381
11. Pedersen, B. K., and Febbraio, M. A. (2008) Muscle as an endocrine organ: focus on muscle-derived interleukin-6. *Physiol. Rev.* **88,** 1379–1406
12. Pedersen, B. K., Akerstrom, T. C., Nielsen, A. R., and Fischer, C. P. (2007) Role of myokines in exercise and metabolism. *J. Appl. Physiol.* **103,** 1093–1098
13. Chan, C. Y., Masui, O., Krakovska, O., Belozerov, V. E., Voisin, S., Ghanny, S., Chen, J., Moyez, D., Zhu, P., Evans, K. R., McDermott, J. C., and Siu, K. W. (2011) Identification of differentially regulated secretome components during skeletal myogenesis. *Mol. Cell. Proteomics* **10,** M110 004804
14. Pedersen, B. K. (2009) Edward F. Adolph distinguished lecture: muscle as an endocrine organ: IL-6 and other myokines. *J. Appl. Physiol.* **107,** 1006–1014
15. Yoon, J. H., Kim, J., Song, P., Lee, T. G., Suh, P. G., and Ryu, S. H. (2012) Secretomics for skeletal muscle cells: a discovery of novel regulators? *Adv. Biol. Regul.* **52,** 340–350
16. Yoon, J. H., Yea, K., Kim, J., Choi, Y. S., Park, S., Lee, H., Lee, C. S., Suh, P. G., and Ryu, S. H. (2009) Comparative proteomic analysis of the insulin-induced L6 myotube secretome. *Proteomics* **9,** 51–60
17. Yoon, J. H., Song, P., Jang, J. H., Kim, D. K., Choi, S., Kim, J., Ghim, J., Kim, D., Park, S., Lee, H., Kwak, D., Yea, K., Hwang, D., Suh, P. G., and Ryu, S. H. (2011) Proteomic analysis of tumor necrosis factor-alpha (TNF-alpha)-induced L6 myotube secretome reveals novel TNF-alpha-dependent myokines in diabetic skeletal muscle. *J. Proteome Res.* **10,** 5315–5325
18. Bi, Y., Wu, W., Shi, J., Liang, H., Yin, W., Chen, Y., Tang, S., Cao, S., Cai, M., Shen, S., Gao, Q., Weng, J., and Zhu, D. (2014) Role for sterol regulatory element binding protein-1c activation in mediating skeletal muscle insulin resistance via repression of rat insulin receptor substrate-1 transcription. *Diabetologia* **57,** 592–602
19. Zhang, W., Liu, J., Tian, L., Liu, Q., Fu, Y., and Garvey, W. T. (2013) TRIB3 mediates glucose-induced insulin resistance via a mechanism that requires the hexosamine biosynthetic pathway. *Diabetes* **62,** 4192–4200
20. Frangioudakis, G., Diakanastasis, B., Liao, B. Q., Saville, J. T., Hoffman, N. J., Mitchell, T. W., and Schmitz-Peiffer, C. (2013) Ceramide accumulation in L6 skeletal muscle cells due to increased activity of ceramide synthase isoforms has opposing effects on insulin action to those caused by palmitate treatment. *Diabetologia* **56,** 2697–2701
21. Dalla-Riva, J., Stenkula, K. G., Petrlova, J., and Lagerstedt, J. O. (2013) Discoidal HDL and apoA-I-derived peptides improve glucose uptake in skeletal muscle. *J. Lipid Res.* **54,** 1275–1282
22. Huang, S., Rutkowsky, J. M., Snodgrass, R. G., Ono-Moore, K. D., Schneider, D. A., Newman, J. W., Adams, S. H., and Hwang, D. H. (2012) Saturated fatty acids activate TLR-mediated proinflammatory signaling pathways. *J. Lipid Res.* **53,** 2002–2013
23. Pu, J., Peng, G., Li, L., Na, H., Liu, Y., and Liu, P. (2011) Palmitic acid acutely stimulates glucose uptake via activation of Akt and ERK1/2 in skeletal muscle cells. *J. Lipid Res.* **52,** 1319–1327
24. Pedrioli, P. G. (2010) Trans-proteomic pipeline: a pipeline for proteomic analysis. *Methods Mol. Biol.* **604,** 213–238
25. Keller, A., Eng, J., Zhang, N., Li, X. J., and Aebersold, R. (2005) A uniform proteomics MS/MS analysis platform utilizing open XML file formats. *Mol. Syst. Biol.* **1,** 2005 0017
26. Braisted, J. C., Kuntumalla, S., Vogel, C., Marcotte, E. M., Rodrigues, A. R., Wang, R., Huang, S. T., Ferlanti, E. S., Saeed, A. I., Fleischmann, R. D., Peterson, S. N., and Pieper, R. (2008) The APEX Quantitative Proteomics Tool: generating protein quantitation estimates from LC-MS/MS proteomics results. *BMC Bioinformatics* **9,** 529
27. Petersen, T. N., Brunak, S., von Heijne, G., and Nielsen, H. (2011) SignalP 4.0: discriminating signal peptides from transmembrane regions. *Nat. Methods* **8,** 785–786
28. Bendtsen, J. D., Jensen, L. J., Blom, N., Von Heijne, G., and Brunak, S. (2004) Feature-based prediction of non-classical and leaderless protein secretion. *Protein Eng. Des. Sel.* **17,** 349–356
29. Mathivanan, S., and Simpson, R. J. (2009) ExoCarta: a compendium of exosomal proteins and RNA. *Proteomics* **9,** 4997–5000
30. Wang, P., Bouwman, F. G., and Mariman, E. C. (2009) Generally detected proteins in comparative proteomics–a matter of cellular stress response? *Proteomics* **9,** 2955–2966
31. Petrak, J., Ivanek, R., Toman, O., Cmejla, R., Cmejlova, J., Vyoral, D., Zivny, J., and Vulpe, C. D. (2008) Deja vu in proteomics. A hit parade of repeatedly identified differentially expressed proteins. *Proteomics* **8,** 1744–1749
32. Kosicka, A., Cunliffe, A. D., Mackenzie, R., Zariwala, M. G., Perretti, M., Flower, R. J., and Renshaw, D. (2013) Attenuation of plasma annexin A1 in human obesity. *FASEB J.* **27,** 368–378
33. Pupjalis, D., Goetsch, J., Kottas, D. J., Gerke, V., and Rescher, U. (2011) Annexin A1 released from apoptotic cells acts through formyl peptide receptors to dampen inflammatory monocyte activation via JAK/STAT/SOCS signaling. *EMBO Mol. Med.* **3,** 102–114
34. Dufton, N., Hannon, R., Brancaleone, V., Dalli, J., Patel, H. B., Gray, M., D'Acquisto, F., Buckingham, J. C., Perretti, M., and Flower, R. J. (2010) Anti-inflammatory role of the murine formyl-peptide receptor 2: ligand-specific effects on leukocyte responses and experimental inflammation. *J. Immunol.* **184,** 2611–2619
35. Bena, S., Brancaleone, V., Wang, J. M., Perretti, M., and Flower, R. J. (2012) Annexin A1 interaction with the FPR2/ALX receptor: identification of distinct domains and downstream associated signaling. *J. Biol. Chem.* **287,** 24690–24697
36. Kim, Y., Lee, B. D., Kim, O., Bae, Y. S., Lee, T., Suh, P. G., and Ryu, S. H. (2006) Pituitary adenylate cyclase-activating polypeptide 27 is a functional ligand for formyl peptide receptor-like 1. *J. Immunol.* **176,** 2969–2975
37. Peshavariya, H. M., Taylor, C. J., Goh, C., Liu, G. S., Jiang, F., Chan, E. C., and Dusting, G. J. (2013) Annexin peptide Ac2–26 suppresses TNFalpha-induced inflammatory responses via inhibition of Rac1-dependent NADPH oxidase in human endothelial cells. *PloS One* **8,** e60790
38. Jia, Y., Morand, E. F., Song, W., Cheng, Q., Stewart, A., and Yang, Y. H. (2013) Regulation of lung fibroblast activation by annexin A1. *J. Cell. Physiol.* **228,** 476–484
39. Ouchi, N., Parker, J. L., Lugus, J. J., and Walsh, K. (2011) Adipokines in inflammation and metabolic disease. *Nat. Rev. Immunol.* **11,** 85–97
40. Bizzarro, V., Belvedere, R., Dal Piaz, F., Parente, L., and Petrella, A. (2012) Annexin A1 induces skeletal muscle cell migration acting through formyl peptide receptors. *PloS One* **7,** e48246
41. Bizzarro, V., Petrella, A., and Parente, L. (2012) Annexin A1: novel roles in skeletal muscle biology. *J. Cell. Physiol.* **227,** 3007–3015
42. Guo, W., Wong, S., Xie, W., Lei, T., and Luo, Z. (2007) Palmitate modulates intracellular signaling, induces endoplasmic reticulum stress, and causes apoptosis in mouse 3T3-L1 and rat primary preadipocytes. *Am. J. Physiol. Endocrinol. Metab.* **293,** E576–E586
43. Holland, W. L., Bikman, B. T., Wang, L. P., Yuguang, G., Sargent, K. M., Bulchand, S., Knotts, T. A., Shui, G., Clegg, D. J., Wenk, M. R., Pagliassotti, M. J., Scherer, P. E., and Summers, S. A. (2011) Lipid-induced insulin resistance mediated by the proinflammatory receptor TLR4 requires saturated fatty acid-induced ceramide biosynthesis in mice. *J. Clin. Investig.* **121,** 1858–1870
44. Cacicedo, J. M., Benjachareowong, S., Chou, E., Ruderman, N. B., and Ido, Y. (2005) Palmitate-induced apoptosis in cultured bovine retinal pericytes: roles of NAD(P)H oxidase, oxidant stress, and ceramide. *Diabetes* **54,** 1838–1845
45. Mayer, C. M., and Belsham, D. D. (2010) Palmitate attenuates insulin signaling and induces endoplasmic reticulum stress and apoptosis in hypothalamic neurons: rescue of resistance and apoptosis through adenosine 5′ monophosphate-activated protein kinase activation. *Endocrinology* **151,** 576–585